analytical chemistry

Article

Cite This: Anal. Chem. 2020, 92, 983−990

pubs.acs.org/ac

Simultaneous Unlocking Optoelectronic and Interfacial Properties of C_{60} for Ultrasensitive Immunosensing by Coupling to Metal−Organic Framework

Qing Zhou,[†,§] Guanghui Li,[‡,§] Kaiyang Chen,[†] Hong Yang,[†] Mengran Yang,[†] Yuye Zhang,[†] Yakun Wan,[*,‡] Yanfei Shen,[*,†] and Yuanjian Zhang[*,†]

[†]School of Chemistry and Chemical Engineering, Medical School, Southeast University, Nanjing 211189, China

[‡]Shanghai Novamab Biopharmaceuticals Co., Ltd., Shanghai 201203, China

Supporting Information

ABSTRACT: Due to exceptional electron-accepting ability, light-absorption, and a delocalized conjugated structure, buckminsterfullerene (C_{60}) has attracted fascinating interest in the field of organic solar cells. However, poor delocalization and accumulation of electrons for pristine C_{60} in physiological aqueous solution and difficulties in conjugation with biomolecules limit its extended photovoltaic applications in bioassay. Herein, we reported the noncovalent coupling of C_{60} to an electronically complementary porphyrin-derived metal−organic framework (PCN-224) with carboxyl-group terminals. Such assembly not only offered a friendly interface for bioconjugation but also resulted in a long-range ordering C_{60}@PCN-224 donor−acceptor system that demonstrated an unprecedented photocurrent enhancement up to 10 times with respect to each component. As an example, by further cooperating with Nanobodies, the as-prepared C_{60}@PCN-224 was applied to a photoelectrochemical (PEC) immunosensor for S100 calcium-binding protein B with by far the most promising detection activities. This work may open a new venue to unlock the great potential of C_{60} in PEC biosensing with excellent performances.

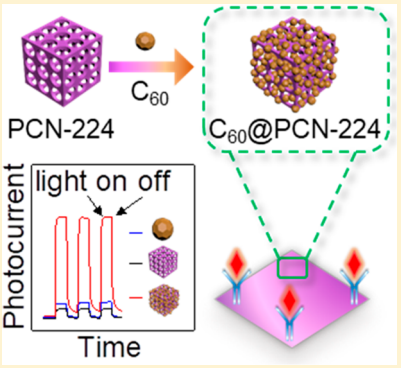

As a promising analytic technique, photoelectrochemical (PEC) immunoassay has received intense attention in the fields of biomarkers detection due to its advantages of low background and high sensitivity, originating from the complete separation of the excitation source and detection signal.[1] It is envisioned that exploring novel photoactive materials with enhanced photoelectric conversion efficiency under physiological aqueous solution would offer an important way to improve the sensitivity of the PEC immunoassay.[2] Up until now, many metal-containing semiconductors such as TiO_2, ZnO, and CdS have been extensively exploited with increasing advances.[3] As a metal-free alternative, C_{60}, has attracted fascinating interests in the field of organic solar cell, due to light-absorption, delocalized conjugated structure, and its superior electron-accepting ability, especially in the excited state.[4] However, there are limited reports on its extended photovoltaic application for a bioassay, ascribing to poor delocalization and accumulation of electrons for pristine C_{60} in a physiological aqueous solution system and the incompatible interface of C_{60} for effective conjugation of biomolecules. To overcome these drawbacks, some interesting strategies were developed. For example, Yuan et al. modified Au nanoparticles on C_{60} to immobilize the capture DNA via Au−S bond for prostate-specific antigen detection.[5] Hu et al. introduced a derivable −COOH group on C_{60} by functionalization with L-cysteine to conjugate biomolecules for screening of thrombin inhibitors.[6] Nevertheless, simultaneous maintaining of the unique optoelectronic properties and endowing of a biofriendly interface for C_{60} is still challenging.

Metal−organic frameworks (MOFs), which are assembled from organic ligand and metal nodes in order, have well-regulated crystalline structures with unprecedented porosity and large specific surface area.[7] The regular porous structure of MOFs allows encapsulating guest molecules to form host−guest nanohybrids.[8] The semiconducting MOFs were also recently reported by using pyrene, porphyrin, or imidazole as the ligand.[9] Also, these MOFs and their derivatives have been applied in the PEC sensor as the photoactive materials.[10] The long-range donor−acceptor (D−A) ordering between electronically complementary MOFs and C_{60} via noncovalent interaction is thereby highly envisioned to be a general favorite scheme to improve transfer of free charge carriers and create novel photoelectrodes with fascinating characteristics.[4c,11] Moreover, by selecting a suitable organic ligand with reactive end-groups, MOFs could also be facilely link to biomolecules. Thus, in principle, by using MOFs as a host and a judicious choice of organic ligand with complementary electronic structure and reactive end-groups, not only the interfacial

Received: August 26, 2019
Accepted: November 19, 2019
Published: November 19, 2019

DOI: 10.1021/acs.analchem.9b03915
Anal. Chem. 2020, 92, 983−990

limitation of C_{60} would be addressed but also the photovoltaic properties of C_{60} could be boosted. Notably, several strategies have been explored to couple MOF and C_{60} for improving the electronic conductivity and charger mobility;[8a,11a,c,d,12] however, few realistic applications are demonstrated. In special, the PEC properties of MOF and C_{60} host−guest system and its great potential in bioassay also has not been explored so far.

Herein, to address the challenge of C_{60} for biosensing in physiological aqueous solution, we report the assembling of C_{60} with porphyrin-derived MOF with carboxyl-group terminals (PCN-224). The carboxyl groups on the highly porous PCN-224 in the assembly (C_{60}@PCN-224) facilitated the conjugation of a large number of biomolecules. Moreover, the long-range ordering D−A interaction between the porphyrin unit in PCN-224 and C_{60} provided an accelerated photoinduced electron transfer for fulfilling an enhanced light harvesting efficiency. As an example, the C_{60}@PCN-224 based PEC immunosensor was successfully constructed by further incorporation of Nanobodies for detecting S100 calcium-binding protein B (S100B), an emerging peripheral biomarker of blood−brain barrier permeability and central nervous system injury, with by far the most promising detection activities.

EXPERIMENTAL SECTION

Materials and Reagents. Tetrakis (4-carboxyphenyl) porphyrin (H_2TCPP) and fullerene C_{60} were purchased from Tokyo Chemical Industry Co., Ltd. (Shanghai, China). Zirconyl chloride octahydrate ($ZrOCl_2 \cdot 8H_2O$) and *p*-benzoquinone was purchased from Aladdin Chemistry Co., Ltd. (Shanghai, China). Glutaraldehyde (GA), dopamine (DA), 1-ethyl-3-(3-(dimethylamino)propyl) carbodiimide hydrochloride (EDC), and *N*-hydroxysuccinimide (NHS) were obtained from Sigma-Aldrich. Dicyandiamide (DCDA) were obtained from Sigma-Aldrich (Germany). Phosphate buffer solutions (PBS) was obtained from Sangon Biotech (Shanghai, China). Bovine serum albumin (BSA) was purchased from Sunshine Biotechnology Co., Ltd. (Nanjing, China). CNQDs was prepared by following the previous work, and the TEM image of CNQDs is shown in Figure S6a.[13] The indium tin oxide (ITO) slices were obtained from Zhuhai Kaivo Optoelectronic Technology Corporation (Zhuhai, China). Benzoic acid, polyvinylpyrrolidone (PVP), *N*,*N*-dimethylformamide (DMF), ethanol, and acetone were purchased from Sinopharm Chemical Reagent Co., Ltd. (Shanghai, China). S100B was purchased from Sino Biological (Beijing, China). The anti-S100B Nanobodies (Nb82 and Nb9) were generated and purified by our own lab (see the detailed method and discussion in the Supporting Information). Freund's complete adjuvant, Freund's incomplete adjuvant, antimouse IgG-alkaline phosphatase, ampicillin, and isopropyl *β*-D-1-thiogalactopyranoside (IPTG) were purchased from Sigma-Aldrich. Mouse anti-HA tag antibody was obtained from Covance Inc. Lymphocyte isolation sterile solution was provided by GE Healthcare. Oligo (dT) primer and 96-well plates were purchased from Thermo Fisher Scientific. *Pst*I and *Not I* were obtained from New England Biolabs Inc. VCSM13 helper phages (Filamentous phage), TG1 cells, and WK6 cells were obtained from Prof. Serge Muyldermans's lab (Laboratory of Cellular and Molecular Immunology, Vrije Universiteit Brussel, Belgium). All reagents were of analytical grade and used as received unless otherwise specified. Ultrapure water (18.2 MΩ cm) was used in all experiments from a Smart2 Pure water purification system (Thermo Fisher).

Preparation of PCN-224 and C_{60}@PCN-224. The PCN-224 was prepared based on the previous report with slight modification.[14] Typically, $ZrOCl_4$ (30 mg), H_2TCPP (20 mg), benzoic acid (1080 mg), and PVP (20 mg) in 3.2 mL of DMF were dissolved in a 10 mL round-bottom flask, followed by heating at 120 °C for 6 h. After cooling down to room temperature, the dark purple cubic crystals were collected via centrifugation and washed with DMF and ethanol. The precipitated PCN-224 was dried at 60 °C for 12 h in a vacuum drier.

To obtain the C_{60}@PCN-224 nanohybrid, C_{60} dispersion (1 mg mL^{-1}, in DMF) was dropped gradually into 1 mL of PCN-224 dispersion (1 mg mL^{-1}, in ethanol) under ultrasonication. Then, the mixture was stirred (800 rpm) overnight. Subsequently, the as-obtained C_{60}@PCN-224 was separated by centrifugation (10 000 rpm, 10 min), after washing with DMF and ethanol. Finally, the precipitate of C_{60}@PCN-224 was redispersed into 1 mL of ethanol and stored under darkness.

Fabrication of Nanobody-Based Photoelectrochemical Immunosensor. For conjugation with Nb82, 1 mL of CNQDs was added into 10 *μ*L of 50% GA solution and then ultrasonicated at room temperature under darkness. After that, 100 *μ*L of Nb82 (100 *μ*g mL^{-1}) in PBS was dropped into the above mixture, and the reaction system was stirred at 4 °C for 12 h. At last, 1% BSA was added and incubated for 1 h to block the nonspecific sites. The as-obtained Nb82@CNQDs was kept away from light at 4 °C before use.

Before the surface modification, the ITO electrodes were gradually washed in acetone, ethanol, and ultrapure water under ultrasonication for 15 min and dried by blowing with high-purity nitrogen gas. Then, the prepared 10 *μ*L of C_{60}@PCN-224 solution was dropped onto the ITO electrode surface and dried in air overnight at room temperature. Afterward, the C_{60}@PCN-224 modified ITO electrode (C_{60}@PCN-224/ITO) was activated by incubating with 10 *μ*L of PBS containing EDC (100 mM) and NHS (50 mM) at 37 °C for 2 h. Subsequently, 10 *μ*L of 10 *μ*g mL^{-1} Nb9 was added onto the surface of C_{60}@PCN-224/ITO and incubated at 4 °C for another 12 h. After rinsing with PBS, the capture Nanobody modified electrode (Nb9/C_{60}@PCN-224/ITO) was blocked by BSA solution (1% w/v in 10 mM PBS), keeping at 37 °C for 0.5 h. After washing, the modified ITO electrode (BSA/Nb9/C_{60}@PCN-224/ITO) was incubated with 10 *μ*L of S100B antigen solution with different concentrations at 37 °C for 2 h, followed by rinsing with PBS. Eventually, 10 *μ*L of above-obtained Nb82@CNQDs dispersion was cast on the modified ITO electrode (S100B/BSA/Nb9/C_{60}@PCN-224/ITO) and incubated at 37 °C for 2 h. The Nanobody-based PEC S100B immunosensor (Nb82@CNQDs/S100B/BSA/Nb9/C_{60}@PCN-224/ITO) was successfully fabricated with rinsing with PBS.

Preparation of Modified Photoelectrodes. In order to measure the performance of photoelectrochemical activity, the photoelectrodes were modified with C_{60}, PCN-224, C_{60}@PCN-224, C_{60}-TCPP, and CNQDs. In detail, the ITO electrodes were cleaned under ultrasonication in acetone, alcohol, and ultrapure water for 15 min, respectively. After blow-drying using high-purity nitrogen gas, 10 *μ*L of 1 mg mL^{-1} dispersion of C_{60}, PCN-224, C_{60}@PCN-224, C_{60}-TCPP, and CNQDs were dropped onto the ITO surface (0.25 cm^2),

DOI: 10.1021/acs.analchem.9b03915
Anal. Chem. 2020, 92, 983−990

respectively. Then, the modified photoelectrodes were dried in air.

Measurement of S100B in Serum Samples. The serum was diluted 100-fold with 10 mM PBS, which was collected from healthy person. Then, the targeted S100B antigen was added into the serum samples to calibrate for 0.5, 1, 5, and 10 ng mL^{-1}, respectively. The spiked serum samples were measured by the above Nanobody-based PEC immunosensor, and each sample was analyzed with three replicates, independently. The concentrations of the serum samples were calculated based on the standard calibration plot.

Apparatus. The photoelectrochemical study was performed on a CHI 600e electrochemical workstation (Shanghai, China) with a Xe lamp (150 W, Beijing NBeT Co., Ltd.) as the source of visible light. The three-electrode system includes a modified ITO electrode with an area of 0.25 cm^2 as the working electrode, an Ag/AgCl (KCl-saturated) electrode as the reference electrode, and a platinum wire as the counter electrode. The electrolyte of PEC study was 10 mM PBS (pH = 6) containing an additional 1 mM DA as the sacrificial agent. The photocurrents were collected at a fixed biased potential (−0.2 V). The transmission electron microscopy (TEM) images were obtained from transmission electron microscopy (JEM-2100, JEM, Japan) and FEI-TF20 TEM systems at an accelerating voltage of 200 kV (FEI). The scanning electron microscopy (SEM) images were measured using a Zeiss Ultra Plus (Germany). The UV−vis absorption spectra were collected using a Cary100 UV−vis spectrophotometer (Agilent, Singapore). The photoluminescence (PL) emission spectra were obtained from a Fluoromax-4 fluorescence spectrometer (Horiba Jobin Yvon, Japan). The time-resolved PL spectra were collected using a PluoroLog 3-TCSPC fluorescence spectrometer (Horiba Jobin Yvon, Japan). Powder X-ray diffraction (XRD) was measured by an Ultima IV X-ray diffractometer (Rigaku, Japan). Nitrogen adsorption−desorption isotherms were collected at 77 K by a Quantachrome Autosorb iQ one-station adsorption instrument. Samples were degassed for 12 h at 120 °C under reduced pressure before measurement.

RESULTS AND DISCUSSION

The general preparation steps for C_{60}@PCN-224 assembly were shown in Figure 1a. Briefly, PCN-224 was first synthesized by heating $ZrOCl_4$ and TCPP in DMF. Then, C_{60} and PCN-224 were facilely coupled in organic solutions, driven by $\pi-\pi$ interaction and physical absorption among them. The morphology of the as-synthesized PCN-224 and C_{60}@PCN-224 was first characterized by SEM. As shown in Figure 1b, the phase-pure PCN-224 exhibited cubic-shape with sharp edges. The SEM and TEM images showed that after coupling to C_{60}, the cubic-shape of PCN-224 was mostly preserved, and some nanoclusters were also observed around the outside surface of the cubes (Figure 1c and 1d).[15] The elemental line scanning analysis of C_{60}@PCN-224 further showed that the elemental Zr mainly distributed in the cube, while the element C was found throughout the whole nanostructure, indicating that the nanoclusters around the cube was also C_{60} (Figure 1e).[16]

To get more structural insights of C_{60}@PCN-224, the porosity and specific surface areas of PCN-224 and C_{60}@PCN-224 were further measured by N_2 adsorption−desorption experiments at 77 K. As shown in Figure 2a, the type-IV isotherm of PCN-224 and C_{60}@PCN-224 were distinctly

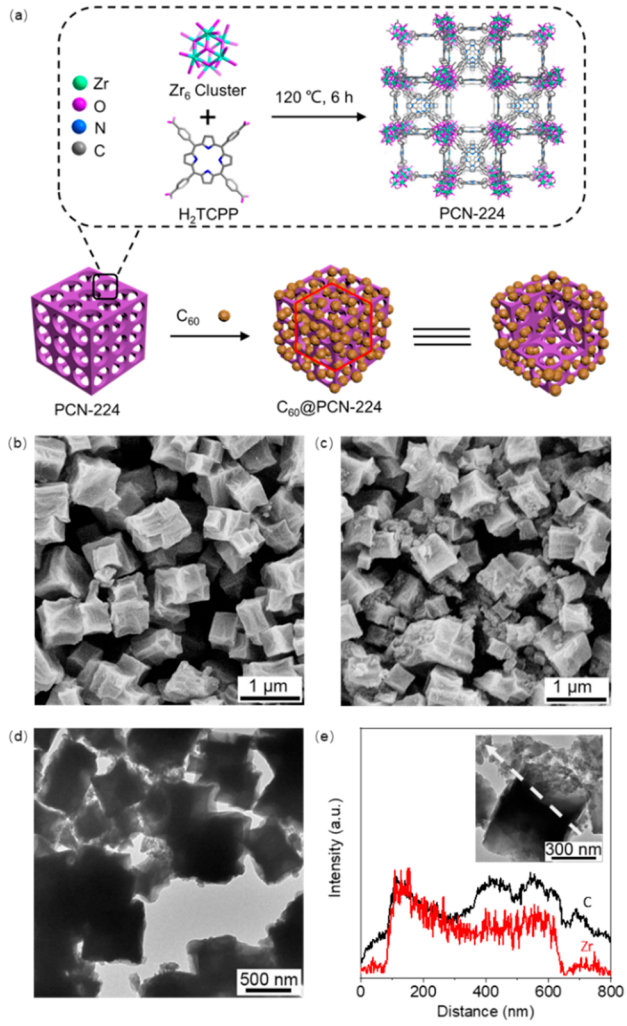

Figure 1. (a) Brief procedure for C_{60}@PCN-224 assembly. SEM images of (b) PCN-224 and (c) C_{60}@PCN-224. (d) TEM image of C_{60}@PCN-224. (e) Elemental line scanning over a single C_{60}@PCN-224 particle indicated by a dashed line in the insert.

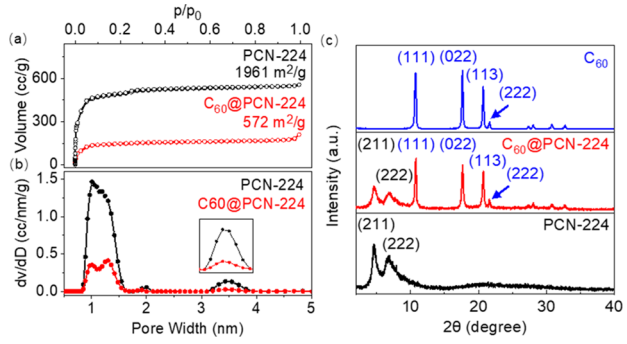

Figure 2. (a) N_2 adsorption−desorption isotherms curves of C_{60}@PCN-224 and PCN-224 (the inset shows the surface area). (b) Density functional theory (DFT) pore size distribution of PCN-224 and C_{60}@PCN-224 obtained from the N_2-adsorption−desorption isotherms in part a. (c) XRD spectra of C_{60}@PCN-224, C_{60}, and PCN-224.

different from each other, and the Brunauer−Emmett−Teller (BET) surface area was calculated to be 1961 m^2 g^{-1} and 572 m^2 g^{-1}, respectively. The density functional theory (DFT) analyses for the pore size distribution indicated the existence of

DOI: 10.1021/acs.analchem.9b03915
Anal. Chem. 2020, 92, 983−990

two types of pores for PCN-224 with sizes of 1.2 nm (triangular microchannels) and 3.5 nm (square mesochannels), respectively.[14] After the assembly with C_{60}, the size of both pores were maintained, while the pore volumes both reduced approximate 80% (Figure 2b), demonstrating that C_{60} was primarily encapsulated in the pores of PCN-224, thanks to the $\pi-\pi$ noncovalent interactions and appropriate pore size matching between PCN-224 host and C_{60} guest.[11c] The X-ray diffraction (XRD) pattern of C_{60}@PCN-224 kept the predominant diffraction peaks from both C_{60} and PCN-224, implying that guest uptake did not alter the crystallinity and also confirming the successful synthesis of C_{60}@PCN-224 (Figure 2c).[17] Therefore, C_{60} was successfully assembled not only on the outer surface of PCN-224, but also encapsulated in the inner micropores to a large extent; meanwhile, the high specific area and high porosity, originated from PCN-244, were fairly retained in the final C_{60}@PCN-224 nanohybrid.

In the second set of experiments, the photoelectrochemical property of C_{60}@PCN-224 was investigated and compared with each single component. For this, the photoelectrodes were prepared by drop-casting of the nanohybrid, PCN-224, or C_{60} onto the ITO. The cross-section SEM of the C_{60}@PCN-224/ITO electrode showed a uniform film could be deposited on the ITO (Figure S2a). The photocurrent response that was measured by a standard photoelectrochemical cell configuration was prompt, steady, and reproducible under the chopped light irradiation (Figure 3a). Nevertheless, it was noted that the photocurrent of PCN-224/ITO and C_{60}/ITO were only 0.88 and 1.17 μA, respectively. In contrast, C_{60}@PCN-224/ITO exhibited a much higher photocurrent up to 9.17 μA, nearly 10 times and 8 times higher than that of PCN-224/ITO and C_{60}/ITO, respectively, indicative of an efficient photocurrent generation by the as-constructed D-Asystem (see more discussion about the effect of exterior and internal C_{60} in Supporting Information). As another control, the photocurrent of C_{60}-TCPP on ITO was also measured to be 1.91 μA, which was merely moderately higher than that of C_{60}. This result showed that the regular porous structure of PCN-224 that led to a desired long ordering assembly of C_{60} played a crucial role in enhancing the photocurrent.

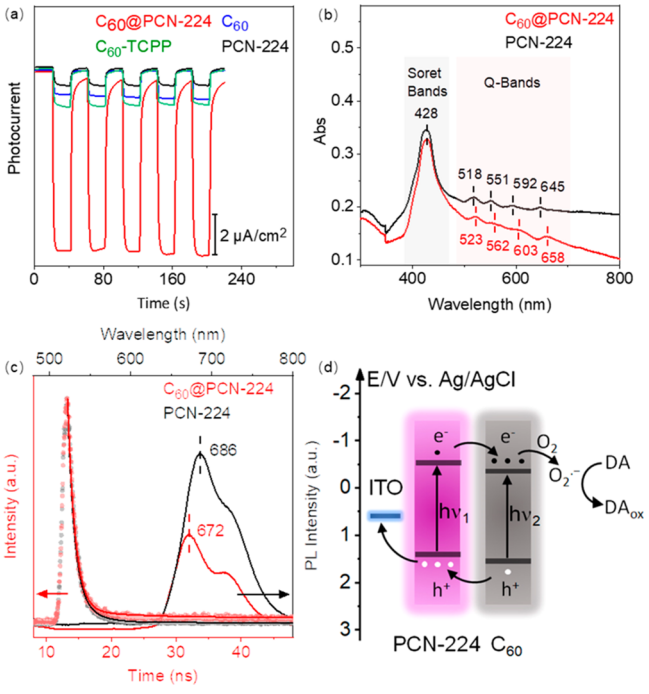

Figure 3. (a) Photocurrent of C_{60}@PCN-224, C_{60}-TCPP, C_{60}, and PCN-224 in 10 mM PBS containing 1 mM DA at a biased potential of −0.2 V. (b) UV−vis spectra of C_{60}@PCN-224 and PCN-224. (c) PL spectra and time-resolved PL spectra of C_{60}@PCN-224 (τ_1 = 1.14 ns, τ_2 = 8.91 ns) and PCN-224 (τ_1 = 0.98 ns, τ_2 = 2.72 ns). (d) Proposed charge transfer mechanism of photocurrent generation of C_{60}@PCN-224.

As the proportion of C_{60} and PCN-224 in C_{60}@PCN-224 was supposed to be an important factor in influencing the photocurrent generation of C_{60}@PCN-224, which would further influence the sensitivity in PEC sensing, the effect of the mass ratio of C_{60} and PCN-224 in the nanohybrid on the photocurrent response of C_{60}@PCN-224/ITO was further examined. As shown in Figure S2b, the photocurrent of C_{60}@PCN-224 improved gradually with the increase of the mass ratio of C_{60} and PCN-224 until the ratio reached 1:1. When further increasing the ratio, the photocurrent started to reduce. Thus, a ratio of 1:1 for C_{60}/ PCN-224 was selected for the preparation of C_{60}@PCN-224 in the following studies.

To further get an insight into the photoexcitation process of the C_{60}@PCN-224 nanohybrid, UV−vis absorption and photoluminescence (PL) spectra were analyzed. As shown in Figure 3b, C_{60}@PCN-224 and PCN-224 both involved a strong absorption peak at 428 nm and four weak absorption peaks in the 500−700 nm region, which could be attributed to the TCPP Soret band and Q-bands.[18] These absorption bands arose from $\pi-\pi^*$ electronic transitions, corresponding to S_0-S_2 and S_0-S_1 electronic transitions, respectively.[9c,19] More interestingly, the Q-bands of C_{60}@PCN-224 showed a slight red shift, revealing the electron transfer between PCN-244 and C_{60}.[16] As shown in Figure 3c, the PL spectrum of PCN-224 showed an emission peak at 686 nm with a shoulder at 718 nm, on account of the typical S_1-S_0 state transition of TCPP.[20] Nevertheless, the emission spectrum of C_{60}@PCN-224 showed significant quenching of the intensity, demonstrating that the construction of D−A inhibited the fast recombination of the photogenerated charge carriers.[21] Also, the main peak of C_{60}@PCN-224 (672 nm) showed a blue shift, which suggested the charge transfer between PCN-224 and C_{60}.[22] The PL lifetimes of C_{60}@PCN-224 and PCN-224 were further calculated by fitting the decay spectra (Figure 3c). Obviously, the short (τ_1) and long (τ_2) lifetimes of the charge carriers in C_{60}@PCN-224 both increased compared to PCN-224. The prolonged PL lifetime further indicated the inhibition of the fast recombination of photogenerated charge carriers by the D−A structure.[21] According to the above results, the long-ordering D−A between PCN-224 and C_{60} can improve the efficient separation of the photogenerated charge carriers by accelerating photoinduced electron transfer and inhibiting the fast recombination of photogenerated charge carriers.[11b,23] Then the enhanced photoelectrochemical performance of C_{60}@PCN-224 was predominated by forming the long-ordering D−A system, which facilitated the separation of the photogenerated charge carriers.

In order to explore the mechanism of the enhanced photoelectric conversion for the C_{60}@PCN-224 nanohybrid, more controls were studied. As shown in Figure S4a, a minor photocurrent response of C_{60}@PCN-224 was observed in the N_2-saturated PBS. While a 5-fold increment was observed for that in the air-saturated PBS, the photocurrent further increased in the O_2-saturated PBS solution, demonstrating

DOI: 10.1021/acs.analchem.9b03915
Anal. Chem. 2020, 92, 983−990

that oxygen molecules could receive electrons from C_{60}@PCN-224 to generate the superoxide radical ($O_2^{\bullet-}$).[9a,24] To verify this speculation, benzoquinone (BQ) was added to the solution as an $O_2^{\bullet-}$ scavenger. As shown in Figure S4b, the photocurrent of C_{60}@PCN-224/ITO in the presence of 1 mM BQ exhibited a 4 times higher photocurrent than that in absence of BQ, which could be attributed to the consumption of $O_2^{\bullet-}$. These results indicated that in the photoexcitation process, oxygen molecules received electrons from C_{60}@PCN-224, generating the superoxide radical ($O_2^{\bullet-}$).[25] Furthermore, the effect of $O_2^{\bullet-}$ depletion agents on the photocurrent of C_{60}@PCN-224/ITO was also explored. As shown in Figure S5, the photocurrent of C_{60}@PCN-224/ITO with DA was much higher than others, demonstrating that DA could be the efficient depletion agent of $O_2^{\bullet-}$ by greatly promoting the generation of photocurrent. Based on the above results, the mechanism which explained the enhanced photocurrent of C_{60}@PCN-224/ITO in 10 mM PBS containing additional 1 mM DA was proposed. As shown in Figure 3d, when C_{60}@PCN-224 was irradiated, both C_{60} and PCN-224 components absorbed photons. The excited electrons transferred from the highest occupied molecular orbital (HOMO) to the lowest unoccupied molecular orbital (LUMO), leaving behind the positive holes in the HOMO.[14,26] Due to the more negative LUMO of PCN-224, the excited electrons of PCN-224 transferred to C_{60}. Then, the electrons in the LUMO of C_{60} moved into the electrolyte, making the O_2 to produce $O_2^{\bullet-}$, which was consumed by DA. Meanwhile, the excited holes of C_{60} transferred to PCN-224, and the HOMO of PCN-224 were scavenged by electrons from ITO. In this context, C_{60} and PCN-224 could construct a D−A system, which suppressed the recombination of charge carriers and accelerated the migration of electron, inducing a high photoelectric conversion efficiency of the C_{60}@PCN-224 nanohybrid. Thus, by coupling to PCN-224, the photoelectrochemical activity of C_{60} was much elevated, which was highly desirable for the construction of a highly sensitive PEC biosensor.

In this report, by taking S100B as a proof-of-concept analyte, a PEC immunoassay with C_{60}@PCN-224 as a probe was developed. S100B is an acidic calcium-binding protein and is primarily expressed and secreted by astrocytes. The level of S100B is normally low in a healthy person and is highly elevated in the serum of patients with a brain injury.[27] For such a reason, S100B has been recognized as an emerging biomarker for brain damage and blood-brain barrier function. Up to date, S100B is generally detected by an enzyme linked immunosorbent assay (ELISA).[28] Despite the advantage in wide application and fast development, the commercial ELISA kits are cost-prohibitive and time-consuming in practical detection.[29] Therefore, it is of significant importance to develop lower-cost, more practicable, and highly efficient strategy for the detection of S100B. Nevertheless, only a limited number of innovative methods for detection of S100B have been developed so far, including electrochemical methods (e.g., Osteryoung square-wave voltammetry and differential pulse voltammetry) and optical immunoassay,[30] whose detection performances still need a substantial improvements for the increasing demanding of clinic diagnosis.

Our previous work showed that the direct immunoassay can be applied for detection of the small molecule by using a Nanobody with a small molecular weight (12−15 kDa), avoiding the complicated procedure of the traditional competitive immunoassay by using conventional monoclonal antibody (mAb).[31] Compared with traditional antibodies, Nb has unique physiochemical properties such as high affinity and specificity, high thermal stability, and acid resistance.[32] Thus, the Nanobody, whose molecular weight was only ∼1/10 of that of mAb, was applied as the recognition unit in the PEC immunosensor. Two Nanobodies, Nb9 and Nb82, which were screened out from camel, were used as the capture Nanobody and label Nanobody, respectively. The construction process of the proposed PEC immunosensor was shown in Figure 4a and

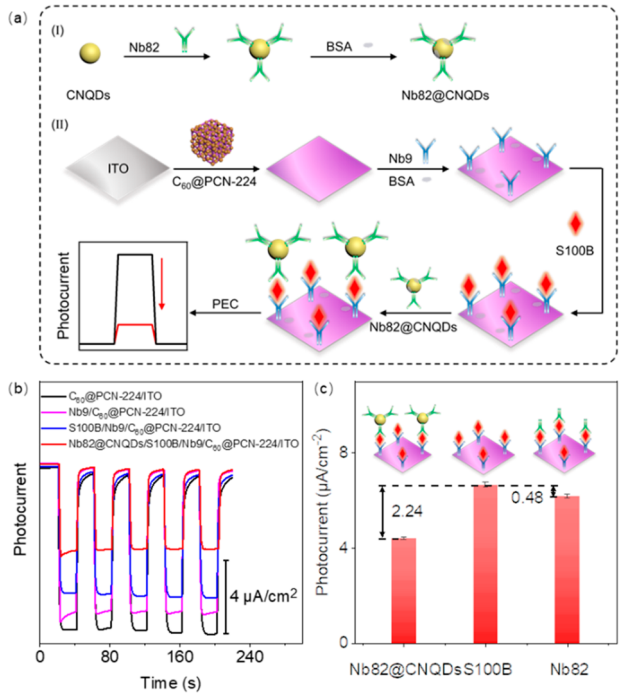

Figure 4. (a) Construction process of S100B PEC immunosensor. (b) Photocurrent of the PEC immunosensor at each assembly step during the fabrication. (c) Photocurrent of the PEC immunosensor in the presence of S100B, Nb82, and Nb82@CNQDs.

confirmed by photocurrent measurement under chopped light irradiation using a standard PEC cell configuration. The photocurrents of all modified electrodes were prompt and reproducible under repeated on/off light irradiation cycles (Figure 4b). As expected, the photocurrent response decreased gradually after incubating C_{60}@PCN-224/ITO with Nb9 and S100B, which could be attributed to the poor conductivity of these protein molecules. Notably, a much more obvious reduction in the photocurrent was observed after the Nb82@CNQDs was captured, which could be ascribed to the quenching effect of the Nb82@CNQDs to C_{60}@PCN-224.

The quenching effect of the Nb82@CNQDs was further confirmed by the comparative study of photocurrent response upon the incubating the photoelectrode (C_{60}@PCN-224/Nb9/BSA/S100B/ITO) with Nb82@CNQDs and Nb82. As shown in Figure 4c, the decrease of the photocurrent upon the incubation of Nb82@CNQDs (ΔI = 2.24 μA) was much larger than that of Nb82 (ΔI = 0.48 μA). Thus, the PEC measurement not only suggested the successful construction of immunosensor but also proved the feasibility of using CNQDs as a PEC quencher for C_{60}@PCN-224.

In order to explain the quenching effect of CNQDs in the as-fabricated PEC immunosensor, the UV−vis absorption was first investigated. As shown in Figure S6b, the CNQDs

DOI: 10.1021/acs.analchem.9b03915
Anal. Chem. 2020, 92, 983−990

exhibited a superior absorption over the ultraviolet region.[13] Nevertheless, the UV−vis spectrum of C_{60}@PCN-224 showed a wide absorption from 300 to 800 nm. There was scarcely any overlap between CNQDs and C_{60}@PCN-224 at the Soret band and Q-bands of C_{60}@PCN-224, which indicated that the competitive absorption of light by CNQDs was not the main factor. To further get an insight into the quenching mechanism of the CNQDs, the PEC performances of CNQDs were investigated. As shown in Figure 5a, the photocurrent of

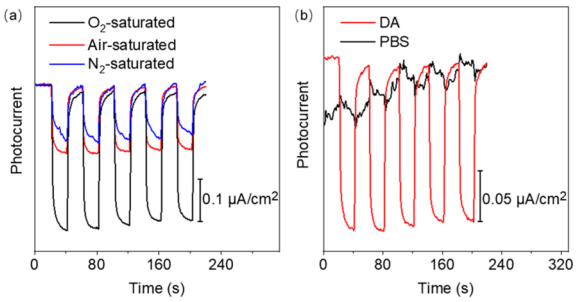

Figure 5. (a) Photocurrent of CNQDs in the air-saturated, N_2-saturated, O_2-saturated PBS solution (10 mM). (b) Photocurrent of CNQDs in the air-saturated 10 mM PBS with and without the addition of 1 mM DA.

CNQDs increased obviously when the amount of O_2 in solution increased, indicating that oxygen molecules could also receive electrons from CNQDs, generating $O_2^{\bullet-}$. Also shown in Figure 5b, the photocurrent of CNQDs with DA was much higher than that in PBS only, demonstrating that DA could also consume $O_2^{\bullet-}$. Thus, similarly with the photoexcitation process of the C_{60}@PCN-224 nanohybrid, the photogenerated electrons of CNQDs were captured by O_2 dissolved in the electrolyte, and the $O_2^{\bullet-}$ could be consumed by the depletion agent (DA). Therefore, the photogenerated electrons of C_{60}@PCN-224 and CNQDs were competitively captured by O_2 dissolved in the electrolyte, and these competitive reactions resulted in the reduced charge carriers separation efficiency of C_{60}@PCN-224, causing lower photocurrent in the presence of CNQDs. Thus, CNQDs, as a competitive-type quencher, improved the sensitivity of this PEC sensor.

As shown in Figure 4a, the Nb82@CNQDs could be quantitatively captured via the immunoreaction, and the photocurrent decrease of C_{60}@PCN-224 would be dependent on the amount of the captured S100B due to the quenching of the CNQDs. Thus, the detection of S100B could be quantified on the difference of the photocurrent decrease after the conjugation of Nb82@CNQDs. As shown in Figure 6a, the photocurrent of the immunosensor reduced gradually with the concentration of target S100B elevated. As displayed in Figure 6b, the change of photocurrent response linearly increased with increasing the logarithm values of S100B concentrations in the range of 1 pg mL^{-1}−100 ng mL^{-1}. The regression equation was expressed as $\Delta I = 0.24 \lg C$ (g mL^{-1}) + 4.40 with a correlation coefficient of 0.9991. The limit of detection (LOD, $3\sigma/S$) for S100B concentration was calculated to be 0.41 pg mL^{-1}, where S is the slope of the calibration curve and σ is the standard deviation of blank samples signals. Compared with a few available methods, the proposed PEC immunosensor showed excellent dynamic sensing range, high-quality correlation coefficient and superior/competitive LOD. In contrast, despite the significant advances, the previous methods

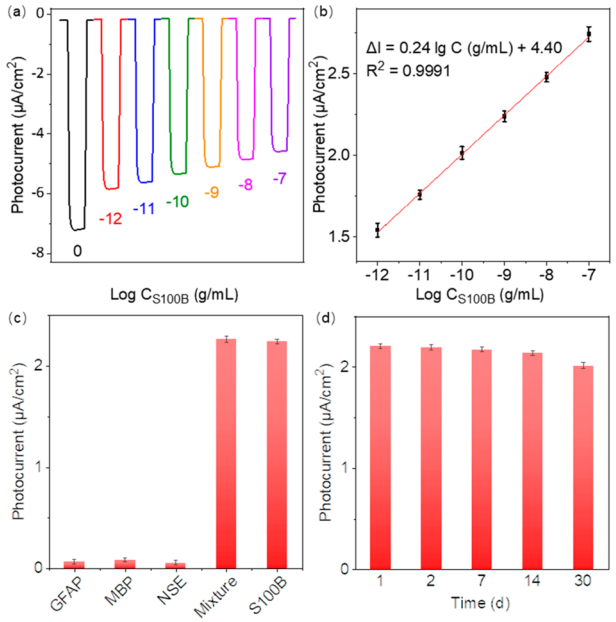

Figure 6. (a) Photocurrent and (b) calibration curve of the PEC immunosensor for detection of the S100B with different concentrations. (c) Selectivity of the proposed PEC immunosensor to 1 ng mL^{-1} S100B by comparing it to the interfering proteins and the mixed sample. (d) Stability of the proposed PEC immunosensor for detecting 1 ng mL^{-1} S100B after 1, 2, 7, 14, and 30 days.

has limitations, either in poor LOD, inadequate correlation coefficient,[30e] or using of heavy metal[30f] which was difficult to apply in practical clinical diagnosis on account of the high environmental toxicity and low biocompatibility (see the detailed comparison in Table 1). Therefore, the C_{60}@PCN-224 was very promising to be applied for an ultrasensitive PEC immunoassay.

To validate the specificity of the PEC immunosensor, the modified photoelectrodes (BSA/Nb9/C_{60}@PCN-224/ITO) were incubated with several typical interfering proteins such as glial fibrillary acidic protein (GFAP), neuron specific enolase (NSE), myelin basic protein (MBP), and the mixture. As shown in Figure 6c, the photocurrent response to GFAP, NSE, and MBP were much lower than that to S100B and the mixture, indicating that these interfering proteins had inappreciable interference to the signal variation. Hence, the proposed PEC immunosensor demonstrated a good selectivity.

Moreover, the stability of the developed immunosensor was evaluated by storing the immunosensor (Nb82@CNQDs/S100B/BSA/Nb9/C_{60}@PCN-224/ITO) in PBS at 4 °C under darkness. As shown in Figure 6d, the constructed immunosensor retained 95.36% of the initial photocurrent response after 2 weeks. Even after 1 month, 89.82% of the initial signal was still maintained, suggesting that the developed immunosensor showed satisfactory stability

The reproducibility of the proposed immunosensor was also evaluated by six parallel experiments in the presence of 1 ng mL^{-1} S100B. As a result, the proposed biosensors showed excellent reproducibility with a relative standard deviation (RSD) of 2.54%. These results revealed that this immunosensor exhibited satisfactory precision and reproducibility. To validate the reliability of this PEC immunosensor, five spiked human serum samples containing different concentrations (0, 0.5, 1, 5, 10 ng mL^{-1}) of S100B were measured. The concentration of S100B was calculated based on the standard

DOI: 10.1021/acs.analchem.9b03915
Anal. Chem. 2020, 92, 983−990

Table 1. Comparison of Sensing Performances of a Few Available Methods for S100B Detection

method	key feature	linear range	correlation coefficient	LOD	refs
ELISA[a]	human S100B ELISA Kit	15.6−1000 pg/mL	N.A.	1 pg/mL	29d
OSWV[b]	pentetic acid complex with Cu(II)	20.96−420 ng/mL	0.945	10.92 ng/mL	30a
OSWV[b]	dipyrromethene complex with Cu(II)	18.9−420 ng/mL	0.9902	18.9 ng/mL	30b
OIA[c]	silicon wafers coated with Si_3N_4	N.A.	0.8	0.25 ng/mL	30c
DPV[d]	potassium ferricyanide redox probe	1 pg/mL−10 ng/mL	0.997	1 pg/mL	30d
DPV[d]	alkaline phosphatase	0.1−100 pg/mL	0.9545	0.1 pg/mL	30e
PEC[e]	CdS quantum dots	0.25−1000 pg/mL	0.9958	0.15 pg/mL	30f
PEC[e]	C_{60}@PCN-224	1 pg/mL−100 ng/mL	0.9991	0.41 pg/mL	this work

[a]Enzyme linked immunosorbent assay. [b]Osteryoung square-wave voltammetry. [c]Optical immunoassay. [d]Differential pulse voltammetry. [e]Photoelectrochemistry.

calibration plot in Figure 6b, and the results were listed in Table S1. The recoveries of all the samples were from 99.79% to 102.41%, with the relative standard deviation (RSD) less than 3.12%, indicating this immunosensor show good reliability for detection of S100B in real serum samples.

CONCLUSION

In summary, C_{60} was successfully coupled to porphyrin-derived MOF (PCN-224) with simultaneously improved optoelectronic and interfacial properties. It was found that the carboxyl-group terminals on PCN-224 provided ample binding sites for highly efficient conjugation of biomolecules. Moreover, the ordered pore channel and high surface area of PCN-224 facilitated C_{60} loading, and the $\pi-\pi$ interaction between porphyrin unit in PCN-224 and C_{60} ensured a long D−A ordering, leading to a tremendously accelerated photoinduced electron transfer, another critical factor for an improved biosensing sensitivity. As an example, the PEC immunosensor by using the proposed C_{60}@PCN-224 nanohybrids as probes and Nanobodies as recognition units was demonstrated for the detection of S100B, exhibiting by far the most promising sensing performances. This work might open new venues for unlocking great potential of C_{60}-based photoelectrodes with biofriendly interface and high photoelectric conversion efficiency in PEC biosensing for early disease diagnosis

ASSOCIATED CONTENT

Supporting Information

The Supporting Information is available free of charge on the ACS Publications Web site. The Supporting Information is available free of charge at https://pubs.acs.org/doi/10.1021/acs.analchem.9b03915.

More experimental procedures; generation of Nanobodies specific to S100B for biosensor fabrication; cross-section SEM image of C_{60}@PCN-224 on ITO and mass ratio optimization of C_{60} and PCN-224 for preparation of C_{60}@PCN-224; photocurrent of C_{60}@PCN-224 in the air-saturated, N_2-saturated, O_2-saturated solution; photocurrent of C_{60}@PCN-224 in the air-saturated PBS consisting additional DA with the absence and presence of BQ; photocurrent of C_{60}@PCN-224 in the air-saturated PBS and consisting additional DA, AA, and cysteine; TEM image, UV−vis absorption spectra, and photocurrent of CNQDs; photocurrent of CNQDs in the air-saturated PBS and consisting additional DA (Figures S1−S6), recovery experiments for sensing S100B in the spiked serum samples from human (Table S1) (PDF)

AUTHOR INFORMATION

Corresponding Authors

*E-mail: Yuanjian.Zhang@seu.edu.cn.
*E-mail: Yanfei.Shen@seu.edu.cn.
*E-mail: ykwan@novamab.com.

ORCID

Yanfei Shen: 0000-0003-0369-5920
Yuanjian Zhang: 0000-0003-2932-4159

Author Contributions

§Q.Z. and G.L. contributed equally. Y.Z. and Y.S. conceived and designed the experiments. Q.Z. prepared and characterized the C60@PCN-224 nanohybrid, fabricated the immunosensor, and performed the sensing experiments. G.L and Y.W. prepared the Nanobodies. K.C., H.Y., M.Y., and Y.Z. contributed to the sensing data collection. All authors contributed to the analysis and discussion of the results. Q.Z., Y.S., and Y.Z. wrote the manuscript, and all authors reviewed the manuscript. Y.S. and Y.Z. supervised the project.

Notes

The authors declare no competing financial interest.

ACKNOWLEDGMENTS

This work was supported by the National Natural Science Foundation of China (Grants 21675022, 21775018, and 81673344), the Natural Science Foundation of Jiangsu Province (Grants BK20170084 and BK20160028), the Fundamental Research Funds for the Central Universities (Grants 2242019K3DN04 and 2242019K41036), and the Postgraduate Research & Innovation Program of Jiangsu Province (Grant KYCX18_0128).

REFERENCES

(1) (a) Haddour, N.; Chauvin, J.; Gondran, C.; Cosnier, S. *J. Am. Chem. Soc.* **2006**, *128* (30), 9693. (b) Zhao, W. W.; Xu, J. J.; Chen, H. Y. *Chem. Soc. Rev.* **2015**, *44* (3), 729.

(2) (a) Zhan, W. W.; Kuang, Q.; Zhou, J. Z.; Kong, X. J.; Xie, Z. X.; Zheng, L. S. *J. Am. Chem. Soc.* **2013**, *135* (5), 1926. (b) Shu, J.; Tang, D. P. *Chem. - Asian J.* **2017**, *12* (21), 2780. (c) Metzger, T. S.; Chandaluri, C. G.; Tel-Vered, R.; Shenhar, R.; Willner, I. *Adv. Funct. Mater.* **2016**, *26* (39), 7148.

(3) (a) O'Regan, B.; Gratzel, M. *Nature* **1991**, *353* (6346), 737. (b) Wang, X. N.; Zhu, H. J.; Xu, Y. M.; Wang, H.; Tao, Y.; Hark, S.; Xiao, X. D.; Li, Q. A. *ACS Nano* **2010**, *4* (6), 3302. (c) Shalom, M.; Ruhle, S.; Hod, I.; Yahav, S.; Zaban, A. *J. Am. Chem. Soc.* **2009**, *131* (29), 9876.

(4) (a) Zhao, G. J.; He, Y. J.; Li, Y. F. *Adv. Mater.* **2010**, *22* (39), 4355. (b) Liu, Y.; Sheri, M.; Cole, M. D.; Yu, D. M.; Emrick, T.; Russell, T. P. *Angew. Chem., Int. Ed.* **2019**, *58* (17), 5677.

DOI: 10.1021/acs.analchem.9b03915
Anal. Chem. 2020, 92, 983−990

(c) Zieleniewska, A.; Lodermeyer, F.; Roth, A.; Guldi, D. M. *Chem. Soc. Rev.* **2018**, *47* (3), 702.
(5) Zhang, Y. H.; Zheng, Y. N.; Li, M. J.; Hu, T.; Yuan, R.; Wei, S. P. *Anal. Chem.* **2018**, *90*, 12278.
(6) Wang, J.; Song, M.; Hu, C.; Wu, K. *Anal. Chem.* **2018**, *90* (15), 9366.
(7) (a) Furukawa, H.; Cordova, K. E.; O'Keeffe, M.; Yaghi, O. M. *Science* **2013**, *341* (6149), 1230444. (b) Lee, J.; Farha, O. K.; Roberts, J.; Scheidt, K. A.; Nguyen, S. T.; Hupp, J. T. *Chem. Soc. Rev.* **2009**, *38* (5), 1450. (c) Zhao, X.; Pachfule, P.; Li, S.; Simke, J. R. J.; Schmidt, J.; Thomas, A. *Angew. Chem., Int. Ed.* **2018**, *57* (29), 8921. (d) Xu, M.; Yuan, S.; Chen, X. Y.; Chang, Y. J.; Day, G.; Gu, Z. Y.; Zhou, H. C. *J. Am. Chem. Soc.* **2017**, *139* (24), 8312.
(8) (a) Chae, H. K.; Siberio-Perez, D. Y.; Kim, J.; Go, Y.; Eddaoudi, M.; Matzger, A. J.; O'Keeffe, M.; Yaghi, O. M. *Nature* **2004**, *427* (6974), 523. (b) An, J. Y.; Shade, C. M.; Chengelis-Czegan, D. A.; Petoud, S.; Rosi, N. L. *J. Am. Chem. Soc.* **2011**, *133* (5), 1220. (c) Jiao, L.; Wang, Y.; Jiang, H. L.; Xu, Q. *Adv. Mater.* **2018**, *30* (37), 1703663. (d) Lu, G.; Li, S. Z.; Guo, Z.; Farha, O. K.; Hauser, B. G.; Qi, X. Y.; Wang, Y.; Wang, X.; Han, S. Y.; Liu, X. G.; DuChene, J. S.; Zhang, H.; Zhang, Q. C.; Chen, X. D.; Ma, J.; Loo, S. C. J.; Wei, W. D.; Yang, Y. H.; Hupp, J. T.; Huo, F. W. *Nat. Chem.* **2012**, *4* (4), 310. (e) Wang, Z.; Zhu, C.-Y.; Mo, J.-T.; Fu, P.-Y.; Zhao, Y.-W.; Yin, S.-Y.; Jiang, J.-J.; Pan, M.; Su, C.-Y. *Angew. Chem. Int. Ed.* **2019**, *131* (29), 9854−9859. (f) Xu, Y.; Tu, W. G.; Zhang, B. W.; Yin, S. M.; Huang, Y. Z.; Kraft, M.; Xu, R. *Adv. Mater.* **2017**, *29* (11), 1605957. (g) Zheng, H.; Zhang, Y.; Liu, L.; Wan, W.; Guo, P.; Nystrom, A. M.; Zou, X. *J. Am. Chem. Soc.* **2016**, *138* (3), 962. (h) He, L.; Liu, Y.; Liu, J.; Xiong, Y.; Zheng, J.; Liu, Y.; Tang, Z. *Angew. Chem., Int. Ed.* **2013**, *52* (13), 3741.
(9) (a) Zhang, G. Y.; Zhuang, Y. H.; Shan, D.; Su, G. F.; Cosnier, S.; Zhang, X. J. *Anal. Chem.* **2016**, *88* (22), 11207. (b) Feng, D.; Gu, Z. Y.; Li, J. R.; Jiang, H. L.; Wei, Z.; Zhou, H. C. *Angew. Chem., Int. Ed.* **2012**, *51* (41), 10307. (c) Lu, K.; He, C.; Lin, W. *J. Am. Chem. Soc.* **2014**, *136* (48), 16712.
(10) (a) Meng, L. X.; Li, Y. M.; Yang, R. Y.; Zhang, X. H.; Du, C. C.; Chen, J. H. *Chem. Commun.* **2019**, *55* (15), 2182. (b) Yang, R. Y.; Zou, K.; Li, Y. M.; Meng, L. X.; Zhang, X. H.; Chen, J. H. *Anal. Chem.* **2018**, *90* (15), 9480.
(11) (a) Goswami, S.; Ray, D.; Otake, K. I.; Kung, C. W.; Garibay, S. J.; Islamoglu, T.; Atilgan, A.; Cui, Y.; Cramer, C. J.; Farha, O. K.; Hupp, J. T. *Chem. Sci.* **2018**, *9* (19), 4477. (b) Zhu, P. H.; Wang, P. P.; Kan, T. L.; Sun, G. Q.; Zhang, Y.; Yu, J. H. *Biosens. Bioelectron.* **2015**, *68*, 604. (c) Dogru, M.; Handloser, M.; Auras, F.; Kunz, T.; Medina, D.; Hartschuh, A.; Knochel, P.; Bein, T. *Angew. Chem., Int. Ed.* **2013**, *52* (10), 2920. (d) Liu, X.; Kozlowska, M.; Okkali, T.; Wagner, D.; Higashino, T.; Brenner-WeiSs, G.; Marschner, S. M.; Fu, Z.; Zhang, Q.; Imahori, H.; Brase, S.; Wenzel, W.; Woll, C.; Heinke, L. *Angew. Chem., Int. Ed.* **2019**, *58*, 9590.
(12) (a) Li, H. Q.; Hill, M. R.; Huang, R. H.; Doblin, C.; Lim, S.; Hill, A. J.; Babarao, R.; Falcaro, P. *Chem. Commun.* **2016**, *52* (35), 5973. (b) Chen, L.; Furukawa, K.; Gao, J.; Nagai, A.; Nakamura, T.; Dong, Y. P.; Jiang, D. L. *J. Am. Chem. Soc.* **2014**, *136* (28), 9806.
(13) Yang, M.; Mei, H.; Shen, Y.; Wu, K.; Pan, D.; Liu, S.; Zhang, T.; Zhang, Y. *Chem. - Eur. J.* **2019**, *25*, 10188.
(14) Chen, Y. Z.; Wang, Z. U.; Wang, H.; Lu, J.; Yu, S. H.; Jiang, H. L. *J. Am. Chem. Soc.* **2017**, *139* (5), 2035.
(15) Xu, H.-Q.; Wang, K.; Ding, M.; Feng, D.; Jiang, H.-L.; Zhou, H.-C. *J. Am. Chem. Soc.* **2016**, *138* (16), 5316.
(16) Zhou, Q.; Xue, H.; Zhang, Y.; Lv, Y.; Li, H.; Liu, S.; Shen, Y.; Zhang, Y. *ACS Sens* **2018**, *3* (7), 1385.
(17) Park, J.; Jiang, Q.; Feng, D.; Mao, L.; Zhou, H. C. *J. Am. Chem. Soc.* **2016**, *138* (10), 3518.
(18) Wang, K.; Yang, J.; Feng, L.; Zhang, Y.; Liang, L.; Xing, W.; Liu, C. *Biosens. Bioelectron.* **2012**, *32* (1), 177.
(19) Aly, S. M.; Ahmed, G. H.; Shaheen, B. S.; Sun, J.; Mohammed, O. F. *J. Phys. Chem. Lett.* **2015**, *6* (5), 791.
(20) Yang, J.; Wang, Z.; Hu, K.; Li, Y.; Feng, J.; Shi, J.; Gu, J. *ACS Appl. Mater. Interfaces* **2015**, *7* (22), 11956.
(21) Wang, J.; Chen, Y.; Shen, Y.; Liu, S.; Zhang, Y. *Chem. Commun.* **2017**, *53* (20), 2978.
(22) Guldi, D. M.; Rahman, G. M. A.; Sgobba, V.; Kotov, N. A.; Bonifazi, D.; Prato, M. *J. Am. Chem. Soc.* **2006**, *128* (7), 2315.
(23) Ohkubo, K.; Kawashima, Y.; Sakai, H.; Hasobe, T.; Fukuzumi, S. *Chem. Commun.* **2013**, *49* (40), 4474.
(24) Schlettwein, D.; Jaeger, N. I.; Wohrle, D. *Ber. Bunsen. Phys. Chem.* **1991**, *95* (11), 1526.
(25) Zhao, Y.; Zhang, Y.; Liu, A.; Wei, Z.; Liu, S. *ACS Appl. Mater. Interfaces* **2017**, *9* (4), 4006.
(26) Shen, Y.; Saeki, A.; Seki, S.; Lee, J.-O.; Aimi, J.; Nakanishi, T. *Adv. Opt. Mater.* **2015**, *3* (7), 925.
(27) (a) Cevik, S.; Ozgenc, M. M.; Guneyk, A.; Evran, S.; Akkaya, E.; Calis, F.; Katar, S.; Soyalp, C.; Hanimoglu, H.; Kaynar, M. Y. *Clin Neurol Neurosur* **2019**, *183*, 105380. (b) Pelinka, L. E.; Kroepfl, A.; Leixnering, M.; Buchinger, W.; Raabe, A.; Redl, H. *J. Neurotraum* **2004**, *21* (11), 1553.
(28) (a) Nylen, K.; Ost, M.; Csajbok, L. Z.; Nilsson, I.; Hall, C.; Blennow, K.; Nellgard, B.; Rosengren, L. *Acta Neurochir.* **2008**, *150* (3), 221. (b) Goncalves, C.-A.; Concli Leite, M.; Nardin, P. *Clin. Biochem.* **2008**, *41* (10−11), 755.
(29) (a) Arya, S. K.; Estrela, P. *Sensors* **2018**, *18* (7), 2010. (b) Pierangeli, S. S.; Harris, E. N. *Nat. Protoc.* **2008**, *3* (5), 840. (c) Jiao, L.; Yan, H.; Xu, W.; Wu, Y.; Gu, W.; Li, H.; Du, D.; Lin, Y.; Zhu, C. *Anal. Chem.* **2019**, *91* (13), 8461. (d) http://www.ptgcn.com/products/Human-S100B-ELISA-Kit-KE00103.htm.
(30) (a) Mikula, E.; Wyslouch-Cieszynska, A.; Zhukova, L.; Puchalska, M.; Verwilst, P.; Dehaen, W.; Radecki, J.; Radecka, H. *Sensors* **2014**, *14* (6), 10650. (b) Kurzatkowska, K.; Jankowska, A.; Wysłouch-Cieszyńska, A.; Zhukova, L.; Puchalska, M.; Dehaen, W.; Radecka, H.; Radecki, J. *J. Electroanal. Chem.* **2016**, *767*, 76. (c) Ettinger, A.; Laumark, A. B.; Ostroff, R.; Brundell, J.; Baumgartner, W. A.; Razumovsky, A. Y. *Ann. Thorac. Surg.* **1999**, *68*, 2196. (d) Khetani, S.; Aburashed, R.; Singh, A.; Sen, A.; Sanati-Nezhad, A. *Sens. Actuators, B* **2017**, *247*, 163. (e) Liu, Y.; Wang, H.; Chen, J.; Liu, C.; Li, W.; Kong, J.; Yang, P.; Liu, B. *Electroanalysis* **2013**, *25* (4), 1050. (f) Tabrizi, M. A.; Ferre-Borrull, J.; Kapruwan, P.; Marsal, L. F. *Microchim. Acta* **2019**, *186* (2), 117.
(31) (a) Li, G. H.; Zhu, M.; Ma, L.; Yan, J. R.; Lu, X. L.; Shen, Y. F.; Wan, Y. K. *ACS Appl. Mater. Interfaces* **2016**, *8* (22), 13830. (b) Zhou, Q.; Li, G.; Zhang, Y.; Zhu, M.; Wan, Y.; Shen, Y. *Anal. Chem.* **2016**, *88* (19), 9830. (c) Pan, D.; Li, G. H.; Hu, H. Z.; Xue, H. J.; Zhang, M. M.; Zhu, M.; Gong, X.; Zhang, Y. J.; Wan, Y. K.; Shen, Y. F. *Chem. - Eur. J.* **2018**, *24* (39), 9869.
(32) Zhang, M.; Li, G.; Zhou, Q.; Pan, D.; Zhu, M.; Xiao, R.; Zhang, Y.; Wu, G.; Wan, Y.; Shen, Y. *ACS Sens.* **2018**, *3*, 684.

DOI: 10.1021/acs.analchem.9b03915
Anal. Chem. 2020, 92, 983−990